Journal of Electronic Materials (2024) 53:5894–5903
https://doi.org/10.1007/s11664-024-11059-z

28TH INTERNATIONAL CONFERENCE ON NUCLEAR TRACKS AND RADIATION MEASUREMENTS

Synergistic Effect of Electrolytes on the Electrochemical Performance of $CoFe_2O_4$ Nanoparticles as Anode Materials for Supercapacitor Applications

Shalendra Kumar[1] · Adil Alshoaibi[2] · Ravina[3] · Kavita Kumari[4] · Faheem Ahmed[5] · Nagih M. Shaalan[2,6] · Saurabh Dalela[7] · Rajesh Kumar[8] · P. A. Alvi[3]

Received: 14 January 2024 / Accepted: 18 March 2024 / Published online: 20 April 2024

Abstract

This article describes the synthesis of $CoFe_2O_4$ nanoparticles, which can be used to form an anode for supercapacitor applications. The $CoFe_2O_4$ nanoparticles were synthesized via a hydrothermal route. The structural parameters of the prepared samples were characterized by x-ray diffraction (XRD) and field-emission scanning electron microscopy (FE-SEM), and the supercapacitive behavior was evaluated by cyclic voltammetry plots, galvanostatic charge–discharge plots, and electrochemical impedance spectroscopy (EIS). Rietveld refinement confirmed the spinel structure of the $CoFe_2O_4$ nanoparticles with space group Fd3m. The FE-SEM micrographs confirmed the spherical shape of the $CoFe_2O_4$ nanoparticles, with a mean particle size of 58 nm. The electrochemical performance of the samples was checked in different aqueous electrolytes: Na_2SO_4 and KOH. The nanoparticles exhibited differences in capacitive behavior in different aqueous electrolytes, with higher specific capacitance (362 F/g) in the KOH electrolyte due to its greater molar ionic conductivity in comparison to the Na_2SO_4, and a low resistance value obtained from impedance measurements was observed for $CoFe_2O_4$ nanoparticles. The cyclic stability of $CoFe_2O_4$ in KOH electrolyte, with 82.16% retention after 2000 cycles at current density of 1 A/g, evidenced its outstanding performance, with exceptionally high specific capacitance of 314 F/g.

Keywords $CoFe_2O_4$ · supercapacitor · impedance spectroscopy · cyclic voltammetry

Introduction

In today's world, the creation of sophisticated energy storage technologies and sustainable energy sources is essential for the advancement of society and research in light of the rising use of fossil fuels.[1–3] Supercapacitors, fuel cells, and batteries are the three primary types of energy conversion and storage technologies. As a result of their superior power density, quick charge–discharge rate, and extended lifetime, supercapacitors have attracted significant research interest.[4] However, the low energy output of supercapacitors in comparison to batteries severely limits the scope of their potential applications.[5] Supercapacitors' ability to store more energy while retaining high power density is becoming more

✉ Shalendra Kumar
shailuphy@gmail.com

1 Department of Physics, School of Advanced Engineering, UPES, Dehradun 248007, India

2 Department of Physics, College of Science, King Faisal University, P.O. Box 400, 31982 Al-Ahsa, Saudi Arabia

3 Department of Physics, Banasthali Vidyapith, Banasthali 304022, India

4 School of Materials Science and Engineering, Changwon National University, Changwon 51140, Gyeongnam, Korea

5 Department of Applied Sciences and Humanities, Faculty of Engineering and Technology, Jamia Millia Islamia, New Delhi 110025, India

6 Physics Department, Faculty of Science, Assiut University, Assiut 71516, Egypt

7 Department of Pure and Applied Physics, University of Kota, Kota, Rajasthan 324005, India

8 University School of Basic and Applied Sciences, Guru Gobind Singh Indraprastha University, New Delhi 110078, India

crucial. The energy density of supercapacitors varies with their capacitance and operating voltage, which is determined by the energy estimation method $E = 1/2CV^2$.[6] Consequently, two methods are frequently utilized to enhance the supercapacitor's energy density by (i) increasing the specific capacitance of electrode materials[7] and (ii) building an asymmetric supercapacitor to increase the cell voltage over a wider range. Carbonaceous materials and transition metal oxides have recently been established in extensive research as electrode materials for supercapacitors.[8] Despite their elevated power density as well as strong cycle stability, carbon-based materials often achieve low capacitance. Alternatively, due to redox reactions occurring at the electrode interface, transition metal oxides generally exhibit higher specific capacitance and excellent energy density. Nevertheless, they have poor cycle stability and rate capacity as a result of their weak conductivity by nature. Therefore, combining these two materials with their respective advantages has emerged as a viable method to enhance the supercapacitor's electrochemical performance.[9]

Transition metal oxides such as WO_3, Fe_2O_3, Co_3O_4, $CoFe_2O_4$, and V_2O_5 have been widely used for ultracapacitors. With its high theoretical capacitance, superior chemical stability, natural abundance, and ecological friendliness, $CoFe_2O_4$ stands out as a potential supercapacitor electrode material.[10] Spinel has recently received significant scientific interest for use in energy applications.[11] With the formula of AB_2O_4 (where A and B represent metal ions), they constitute a category of composite metals with highly versatile properties.[12] The spinel mixed-phase composition of transition metals offers the electrical and catalytic advantages needed for energy storage and conversion. Structured carbons, transition metal oxides, and sulfides are examples of electro-active materials that have previously been investigated for use in batteries, supercapacitors, fuel cells, and water splitting. However, the low stability of transition metal sulfides, low electrical conductivity of transition metal oxides, and low activity of carbon-based materials restrict their suitability for use in future energy devices.[13] In energy conversion or storage applications, transition metal-based systems such as cobalt and iron oxides, hydroxides, and sulfides have recently been investigated.[14–18] However, the electrochemical performance of these materials is not very good. Several studies have indicated that iron and cobalt spinels provide improved electrical conductivity, more active sites, and superior electrochemical performance. As a consequence of their significance to the electronic materials industry, ferrites of the type MFe_2O_4 ($M = Ni^{2+}$, Co^{2+}, Cu^{2+}, etc.) have received increasing attention. Recording heads, transformer cores, memory, microwave device loading coils, and antenna rods are among the most exciting applications nowadays.[19,20] Cobalt ferrite ($CoFe_2O_4$) in particular (magnetic devices) has been employed because of their strong magnetic anisotropy, mild saturation magnetization, chemical stability, mechanical hardness, high coercivity, and magnetostriction.[21] $CoFe_2O_4$ thin films are employed for high-temperature gas sensor applications.[22] $CoFe_2O_4$ has received considerable attention because of its low-cost cycle stability and towering specific capacity.[23,24] Metal compounds, however, have low conductivity, which reduces their superior electrochemical performance when used in electrochemical energy storage systems. This article reports two types of electrolytes used in electric double-layer capacitors (EDLCs): organic and aqueous. Aqueous electrolytes are better than organic electrolytes because of their poor internal resistance, low cost, good conductivity, and non-flammability.[25,26] Na_2SO_4 and KOH are the two types of aqueous electrolytes that are used in this research and have different ionic radii, in particular different hydrated ionic radii. In this work, electrochemical impedance spectroscopy (EIS), cyclic voltammetry (CV), and galvanostatic charge–discharge (GCD) measurements were used to thoroughly evaluate two aqueous electrolytes for supercapacitor applications.

Experimental

To create the $CoFe_2O_4$ nanoparticles, a microwave-assisted hydrothermal process was used. All compounds were of analytical quality, purchased from Sigma-Aldrich, and utilized without additional treatment. In a typical procedure, a solution of cobalt(II) nitrate hexahydrate and iron(III) nitrate nonahydrate in 50 mL deionized (DI) water was dissolved with the help of continuous magnetic stirring. The solution was then made alkaline by introducing NH_4OH in dropwise fashion until pH of 9 was reached. After 1 h of stirring at room temperature, the prepared solution was poured into a Teflon vessel, and its temperature was maintained at 200°C in the microwave for 5 min. After microwave processing, the solution was allowed to cool at room temperature. The precipitate obtained after centrifugation was rinsed five times with DI water and 100% ethanol before being separated by centrifugation at 5000 rpm. Lastly, the precipitate was dried in a hot air oven at ~ 80°C for 2 h. The phase analysis of the resultant product was conducted via x-ray diffraction (XRD) utilizing a Philips X'Pert (MPD-3040) diffractometer with a copper Kα radiation source (λCuK$\alpha = 1.5406$ Å). Field-emission scanning electron microscopy (FE-SEM) was employed for imaging utilizing a MIRA II LMH microscope. The elemental composition of $CoFe_2O_4$ was determined through energy-dispersive x-ray spectroscopy (EDX), facilitated by an

Inca Oxford system integrated with FE-SEM. A 1 M aqueous solution of KOH and Na_2SO_4 was used as the electrolyte for all electrochemical characterizations in a traditional three-electrode cell arrangement. A mixture of 10% carbon black, 10% polyvinylidene fluoride (PVDF), and 80% active materials ($CoFe_2O_4$) were combined to create the working electrodes. In order to create a slurry, the weighted electrode materials were thoroughly combined with *n*-methyl-2 pyrrolidinone (NMP) as a solvent material. The obtained slurry was kept as paste to the ~ 1.0 cm^2 nickel foam substrate and allowed to dry for 12 h at 80°C in a hot air oven. The size and form of each electrode were the same. Pt and Ag/AgCl were used as the reference and counter electrodes, respectively.

Results and Discussion

XRD

The crystalline phase and structure of the $CoFe_2O_4$ nanoparticles were characterized using the XRD technique at room temperature. Figure 1a shows the synthesized sample's XRD pattern. The spinel structure of $CoFe_2O_4$ nanoparticles with space group Fd3m was attributed to the diffraction peaks seen at $2\theta = 29.92°$, 35.34°, 42.9°, 53.58°, 57.43°, and 62.44°, 74.20°, which correspond to the (220), (311), (400), (422), (333), (440), and (533) planes. The XRD pattern was examined using the Rietveld refinement technique and FullProf software, and the results are displayed in Fig. 1a. The black circles and red line represent the data points associated with the experimental and theoretical calculations, respectively. Bragg's positions in relation to the face-centered cubic (FCC) structure are shown by vertical blue lines. The pink line represents the discrepancy between the theoretical and experimental data. The value of χ^2 is 1.02, which illustrates the quality and consistency of the refinement. With lattice parameters of $a = b = c = 8.383$Å, every diffraction peak indexed in the XRD pattern was equivalent to the JCPDS card number 22-1086. The effective synthesis of $CoFe_2O_4$ is demonstrated without any impurity phase. The Debye–Scherrer equation (Eq. 1) is used to estimate the crystalline size[27–30]:

$$D = \frac{K\lambda}{\beta \mathrm{COS}\theta} \tag{1}$$

where θ, β, λ, and K represent Bragg's angle, the full width at half maximum (FWHM), the wavelength of x-rays (on the order of ~ 1.5406 Å), and constant shape factor (~0.9), respectively. The formula in Eq. (1) was utilized to determine the standard crystallite size of $CoFe_2O_4$ nanoparticles and was observed at ~ 35.0 nm. The micro-strain determined using Williamson–Hall (W-H) plots (see Fig. 1b) was ~ 0.2480. The dislocation density can be determined using the formula (2) as follows:

$$\text{Dislocation density}(\delta) = \frac{1}{D^2} \tag{2}$$

where D is the average crystallite size, and $D = 34.92$ nm. Hence, the dislocation density is 8.2×10^{-4}. Interplanar spacing can be calculated with the help of Eq. (3):

$$n\lambda = 2d \sin\theta \tag{3}$$

Here, λ is the wavelength. The calculated value of interplanar spacing is 2.53A° for the high intense peak (311), and the lattice parameter (a) was also calculated using the formula (4)

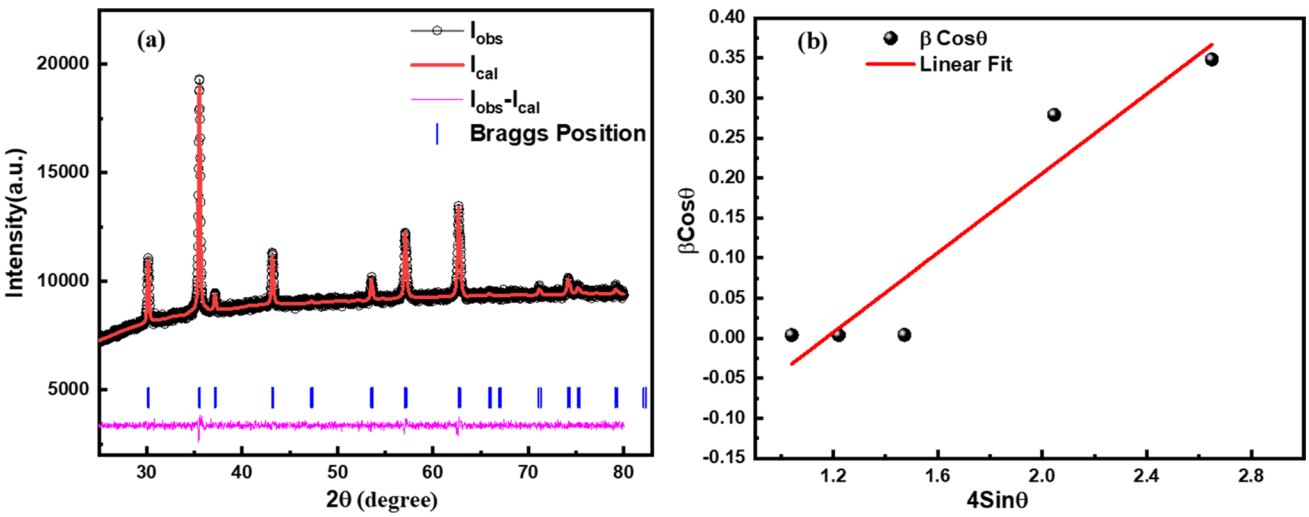

Fig. 1 (a) XRD plot of $CoFe_2O_4$ nanoparticles, (b) W-H plot of $CoFe_2O_4$ nanoparticles.

$$a = \frac{d_{hkl}}{\sqrt{(h^2 + k^2 + l^2)}} \quad (4)$$

Here, (*h, k, l*) represent the Miller indices, whereas d_{hkl} denotes the interplanar spacing determined using the XRD pattern, which is 8.38A°.

SEM

Figure 2a highlights the surface morphology of $CoFe_2O_4$ nanoparticles using FE-SEM. In Fig. 2b, elemental mapping illustrates the distribution of elements within the $CoFe_2O_4$ nanoparticles. The inset of Fig. 2c presents the EDX spectrum of the $CoFe_2O_4$ nanoparticles. The FE-SEM image highlights the nanocrystalline nature and spherical morphology of the $CoFe_2O_4$ nanoparticles. Utilizing ImageJ software, the particle size was determined to be ~ 58 nm, as depicted in Fig. 2d.

Electrochemical Analysis

Cyclic Voltammetry (CV) Study

The electrode performance of the $CoFe_2O_4$ nanoparticles was investigated in different electrolytes Na_2SO_4

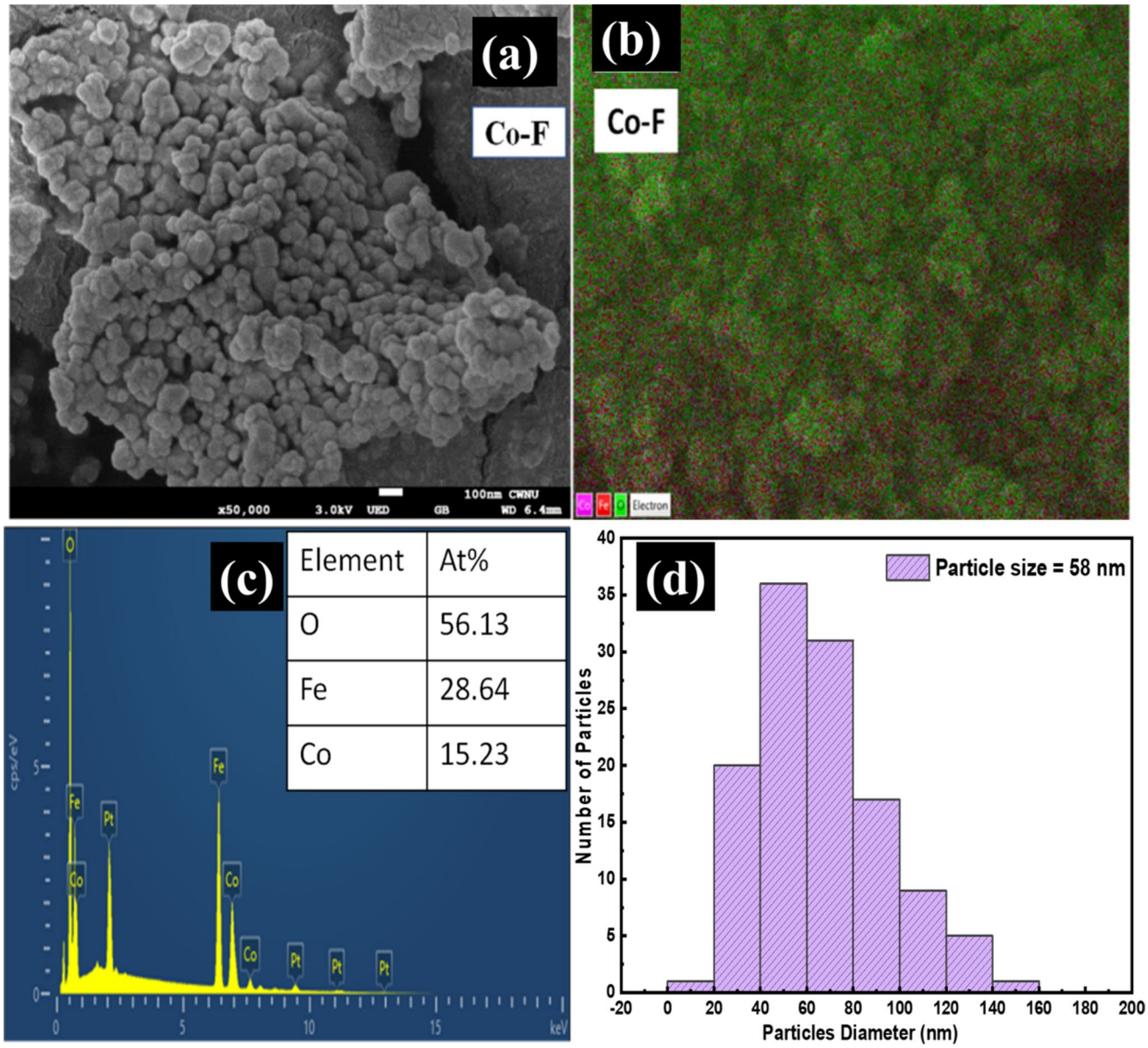

Fig. 2 (a) FE-SEM image of $CoFe_2O_4$ nanoparticles. (b) Elemental mapping of $CoFe_2O_4$ nanoparticles. Inset in (c) highlights the EDS spectrum of $CoFe_2O_4$ nanostructure. (d) Particle size distribution histogram of $CoFe_2O_4$ nanostructure.

and KOH. The CV measurements on the $CoFe_2O_4$ nanoparticles were performed in a traditional three-electrode configuration. Platinum wire was utilized for the counter electrode, while the Ag/AgCl electrode was used as the reference electrode. Electrolyte solutions of 1 M KOH and 1 M Na_2SO_4 were utilized for the electrochemical measurements. The electrode was fabricated using carbon black, polyvinylidene fluoride (PVDF) binder, and active material in a ratio of 10:10:80 in NMP solvent, which was drop-cast onto nickel foam with a mass of approximately 1.5 mg. The nickel foam was allowed to dry for 12 h before testing. Equation (5) was utilized to determine the specific capacitance of the $CoFe_2O_4$ nanoparticles.

$$C = \frac{\int I \cdot \mathrm{d}V}{mk\left(V_2 - V_1\right)} \tag{5}$$

The area covered by the volumetric curve is represented by the integral component in the above formula, the mass of the material is denoted by m, the potential window is represented by the term $(V_2 - V_1)$, which displays the difference between the two voltages, and the scan rate is indicated by k. Figure 3a and c show the CV curves of $CoFe_2O_4$ nanoparticles recorded at scan rates of 10, 20, 50, and 100 mV/s for KOH and Na_2SO_4 electrolytes, respectively. The specific capacitance calculated from the CV curve measured at different scan rates in KOH and Na_2SO_4 electrolytes is depicted in Fig. 3b and d, respectively. It is seen that the CV curves take on a

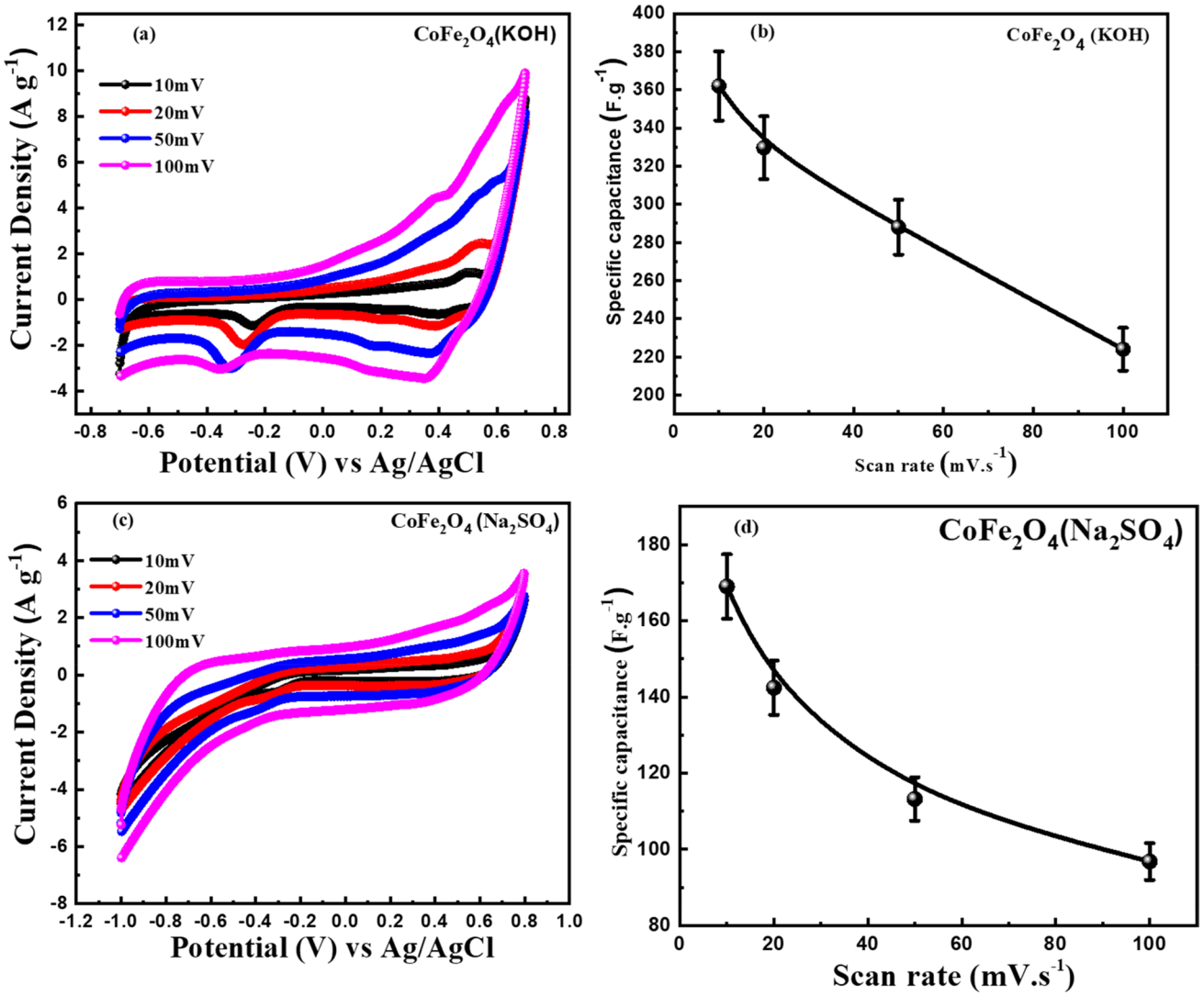

Fig. 3 (a) CV plot of $CoFe_2O_4$ nanoparticles determined in KOH electrolyte at different scan rates, (b) specific capacitance of $CoFe_2O_4$ nanoparticles measured in KOH electrolyte at different scan rates, and (c) CV plot of $CoFe_2O_4$ nanoparticles recorded in Na_2SO_4 electrolyte at different scan rates. (d) Specific capacitance of $CoFe_2O_4$ nanoparticles measured in Na_2SO_4 electrolyte at different scan rates.

somewhat different form, becoming quasi-rectangular. This suggests that the mechanism of charge storage can be controlled by both EDLC and the Faradaic reaction (Fe/Fe^{+2} or Co/Co^{+2}) in the potential range of −0.7 to 0.7 V for the KOH electrolyte and −1.0 to 0.8 V for Na_2SO_4. The $CoFe_2O_4$ electrode demonstrated the highest specific capacitance, approximately 362 F/g, measured in 1 M KOH electrolyte at a scan rate of 10 mV/s. In contrast, in the Na_2SO_4 electrolyte, a specific capacitance of 168.96 F/g was recorded. KOH displayed superior capacitive behavior compared to Na_2SO_4, attributed to its higher mobility, smaller hydrated radius, shorter ionic radius, and greater molar ionic conductivity.[31,32] This difference in electrolyte properties resulted in lower electrochemical impedance. A comparison of the specific capacitance values across the different electrolytes is summarized in Table I.

Table I Specific capacitance of $CoFe_2O_4$ nanoparticles at different KOH and Na_2SO_4 electrolyte scan rates

Scan rate(mV/s)	Specific capacitance (KOH electrolyte)	Specific capacitance (Na_2SO_4 electrolyte)
10	362	168.96
20	329	142.4
50	288	113.2
100	224	96.8

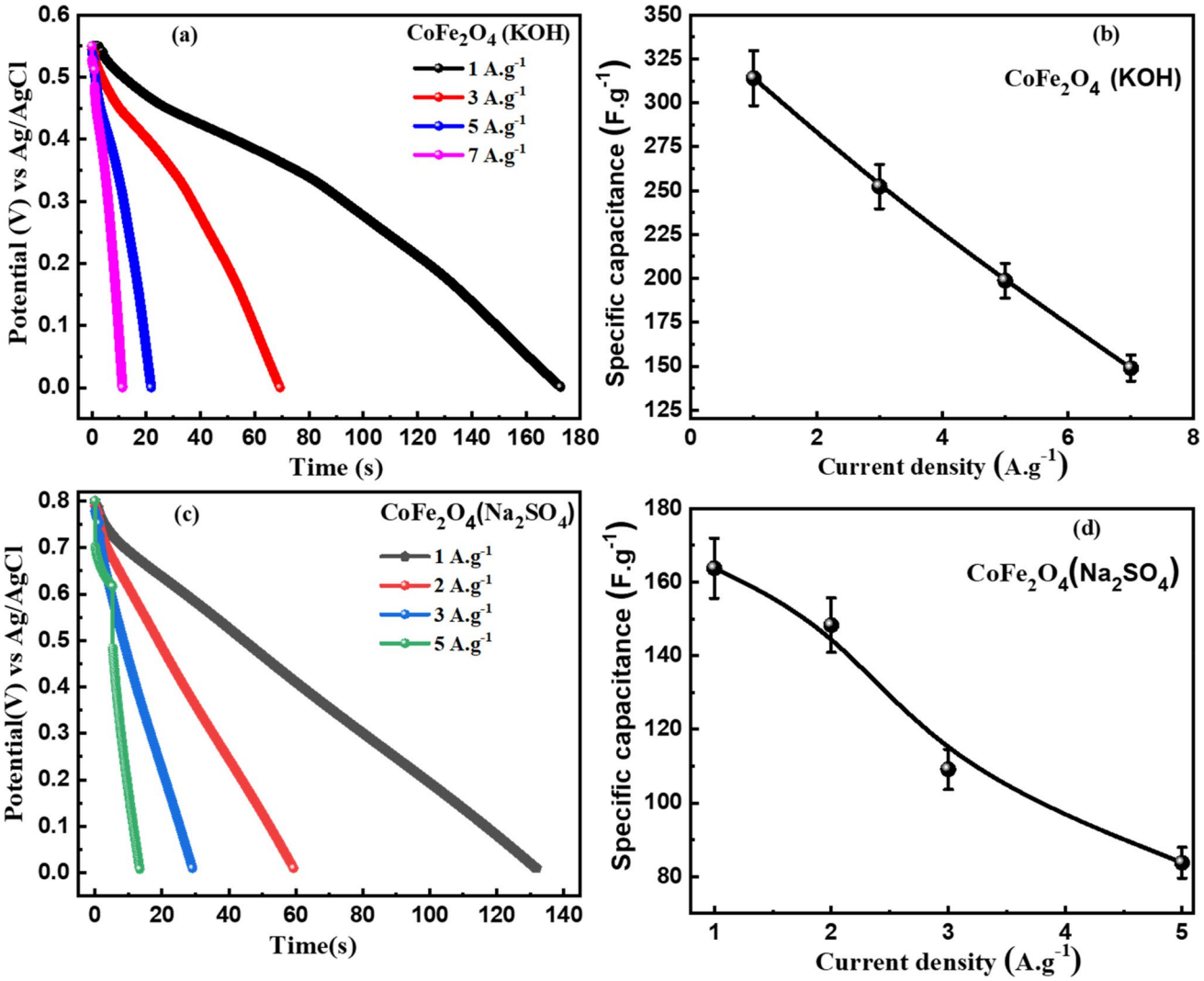

Fig. 4 (a) GCD plot of $CoFe_2O_4$ nanoparticles at different current densities recorded in KOH electrolyte, (b) variation in specific capacitance of $CoFe_2O_4$ nanoparticles at different current densities measured in KOH electrolyte, and (c) GCD plot of $CoFe_2O_4$ nanoparticles at different current densities in Na_2SO_4 electrolyte. (d) Variation in specific capacitance of $CoFe_2O_4$ nanoparticles at different current densities measured in Na_2SO_4 electrolyte.

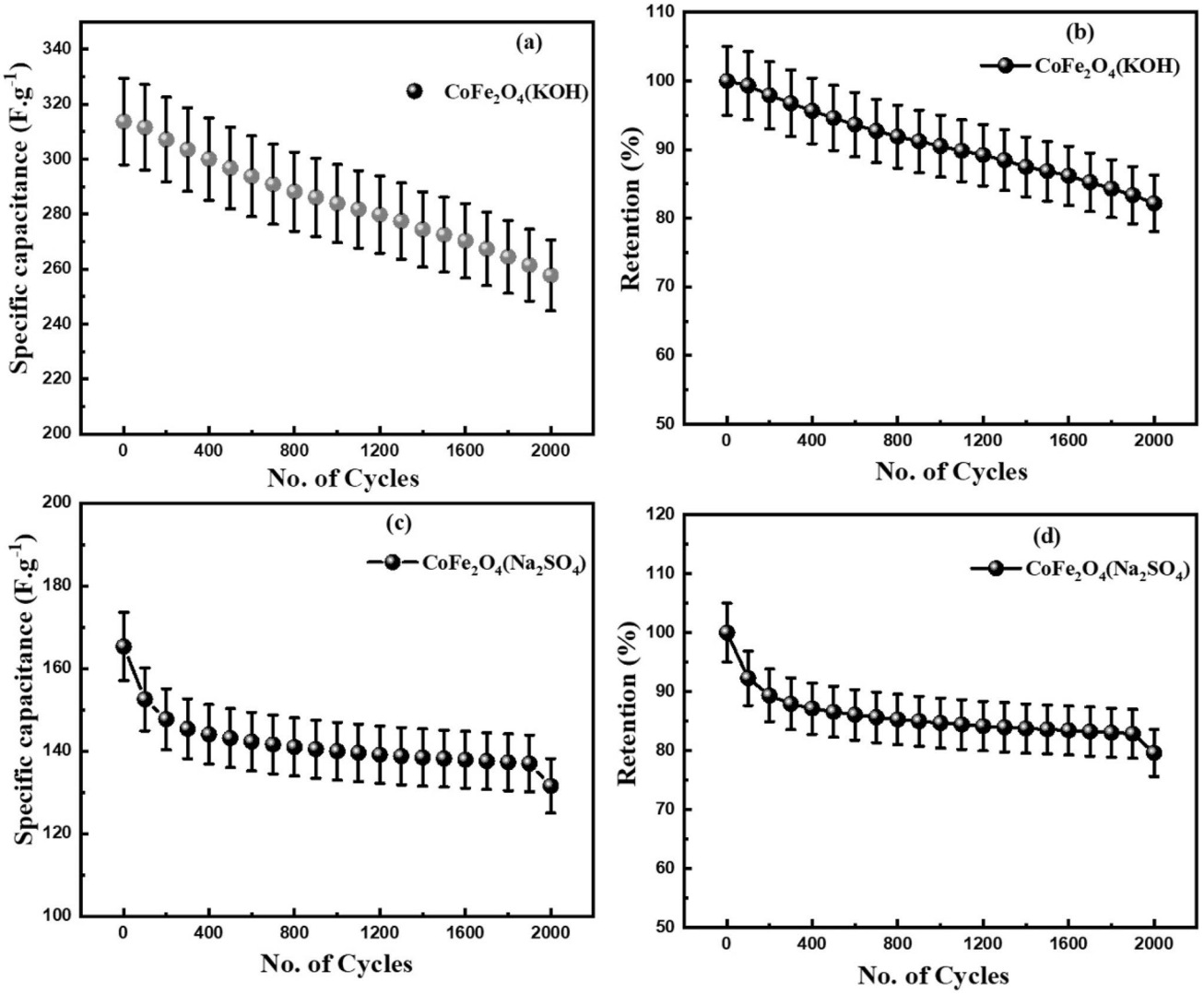

Fig. 5 (a) Cyclic performance of $CoFe_2O_4$ nanoparticles in the KOH electrolyte for 2000 cycles at 1 A/g, (b) plot of retention versus cycle number of $CoFe_2O_4$ nanoparticles recorded in KOH electrolyte, (c) cyclic performance of $CoFe_2O_4$ nanoparticles measured in Na_2SO_4 electrolyte for 2000 cycles at 1 A/g, (d) plot of retention versus cycle number of $CoFe_2O_4$ nanoparticles in Na_2SO_4 electrolyte.

Galvanostatic Charge–Discharge (GCD) Study

GCD curves are crucial for understanding the electrochemical behavior of energy storage devices, aiding in optimizing systems, and guiding advancements in energy storage technology. Figure 4a depicts the GCD curves of the $CoFe_2O_4$ electrode recorded in 1 M KOH at current densities of 1, 3, 5, and 7 A/g in the potential window of 0.0–0.7 V, and Fig. 4c represents the GCD curve of $CoFe_2O_4$ electrode noted in 1 M Na_2SO_4 electrolyte at various current densities of 1, 2, 3, and 5 A/g potential window 0–0.8 V. From the GCD curves, the specific Eq. (6) as given below, was used to compute the value of specific capacitance (C_s):

$$C_s = \frac{I \times \Delta t}{m \cdot \Delta V} \tag{6}$$

where m represents the mass of active material on the electrode, ΔV is the potential window, I (A) is the discharge current, and Δt (s) highlights the duration of discharge time. Compared to $CoFe_2O_4$ (Na_2SO_4) samples, the discharge duration in the GCD curves of $CoFe_2O_4$(KOH) samples is much longer, indicating a substantially higher specific capacitance. Furthermore, the specific capacitance is reduced as the current density increases, as can be seen in Fig. 4b and d. The emergence of inner active sites cannot completely maintain the redox transition at higher current densities, which may be caused by a proton diffusion effect within the electrode. The electrode's active sites can effectively react with

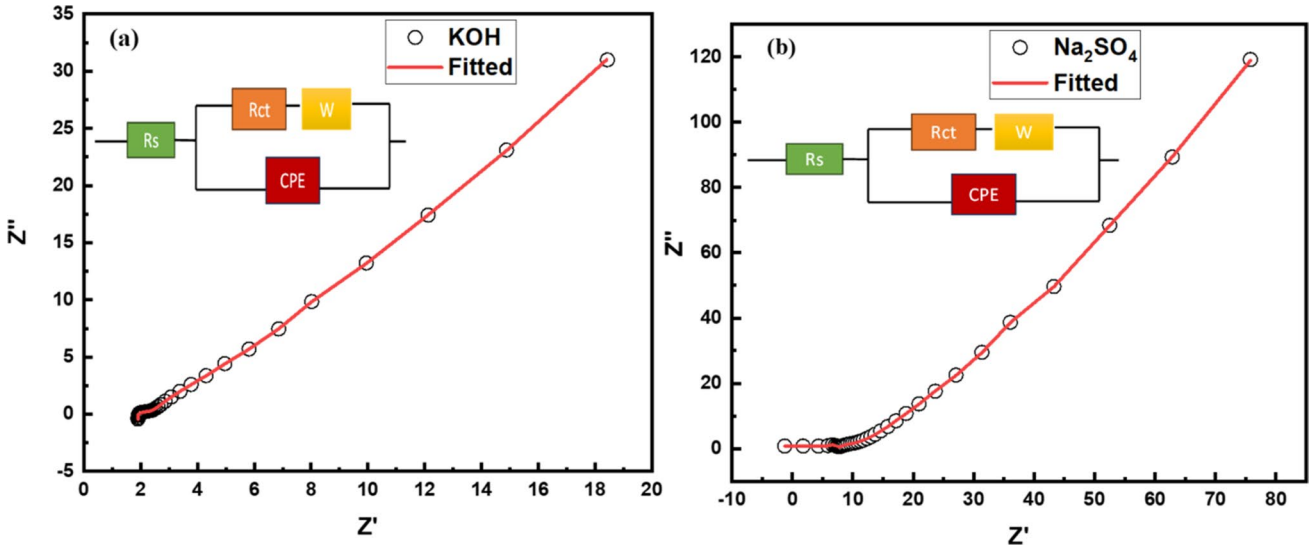

Fig. 6 (a) Nyquist plot of $CoFe_2O_4$ nanoparticles recorded in KOH electrolyte; inset represents the equivalent circuit. (b) Nyquist plot of $CoFe_2O_4$ nanoparticles recorded and measured in Na_2SO_4 electrolyte; the inset shows the equivalent circuit.

Table II Rs and Rct values of $CoFe_2O_4$ nanoparticles for KOH and Na_2SO_4 electrolytes

Element	KOH (electrolyte)	Na_2SO_4 (electrolyte)
Rs	2.297	2.93
Rct	1.134	7.62

the ions in the electrolyte at low current densities. The redox reaction can only occur on the surface of active materials due to the restriction of ion flow in the rapid charge–discharge rate, which results in a loss of specific capacitance. The $CoFe_2O_4$ nanoparticles exhibit a high specific capacitance in the KOH electrolyte compared to the Na_2SO_4 electrolyte, as shown in Fig. 4b and d. The value of the specific capacitance determined at current densities of 1 A/g in KOH and Na_2SO_4 was 314F/g and 163.75F/g, respectively. Therefore, it is evident from Fig. 4b and d that the $CoFe_2O_4$ electrode in the KOH electrolyte performs better electrochemically than the Na_2SO_4) electrolyte, which is better than ferrite supercapacitor electrodes described previously. Figure 5a and c illustrate the testing of the cycling stability of the $CoFe_2O_4$ electrode recorded in the KOH and Na_2SO_4 electrolyte over 2000 cycles at a current density of 1 A/g. Figure 5b and d illustrate the retention rates, which were found to be 82.16% and 79.59% for the $CoFe_2O_4$ electrode in KOH and Na_2SO_4 electrolytes, respectively.

Electrochemical Impedance Spectroscopy (EIS) Study

EIS is a powerful technique for describing the electrochemical performance of supercapacitors. Figure 6a and b show the Nyquist plot $CoFe_2O_4$ for KOH and Na_2SO_4 electrolytes in the frequency range of 0.01 Hz–100 kHz. The impedance is generally a complex number and is represented by $Z = Z' + iZ''$, where Z′ and Z″ are the real and imaginary parts, respectively. In the high-frequency area it displays a semicircular arc, and in the low-frequency region a straight line. The transfer of charge resistance at the electrode–electrolyte interface is represented by the diameter of the semicircle in the high-frequency regime. The equivalent series resistance (ESR) in the high-frequency field is defined by the intersection of the semicircle. The supercapacitor based on $CoFe_2O_4$ (KOH) is shown in Fig. 6a, and $CoFe_2O_4$ (Na_2SO_4) is shown in Fig. 6b, showing a very short kinetic arc at higher frequencies, suggesting the charge transfer regulated behavior, and a straight line at low frequencies showing the capacitive behavior, as validated by the EIS measurement. Table II clearly shows that for $CoFe_2O_4$ with KOH (electrolyte), the values of Rs and Rct are lowest. This indicates that the electrode achieves high capacitance in KOH electrolytes because of the spontaneous electrochemical reaction between the electrolyte and active electrode material due to its large surface areas. Charge migration at the solid–liquid interfaces is made easier by the lower values of Rs and Rct.

Conclusion

The synthesis of $CoFe_2O_4$ nanoparticles was carried out via a hydrothermal process, and their electrochemical performance was investigated in Na_2SO_4 and KOH, the aqueous electrolytes. The structural parameters were

determined using the XRD technique followed by Rietveld refinement, which confirmed the spinel structure with space group Fd3m. The FE-SEM micrographs revealed the spherical shape of the $CoFe_2O_4$ nanoparticles, with an average particle size of 58 nm. Further, the supercapacitive behavior was studied by CV, GCD plots, and EIS spectroscopy. The nanoparticles exhibited dissimilar capacitive behavior in different aqueous electrolytes, signifying the highest specific capacitance (362F/g) in the KOH electrolyte due to its maximum molar ionic conductivity in comparison to the Na_2SO_4, and a low resistance value obtained from impedance measurements was observed for $CoFe_2O_4$ (KOH). The cyclic stability of $CoFe_2O_4$ (KOH), with 82.16% retention after 2000 cycles at a current density of 1 A/g, demonstrates its outstanding performance, with exceptionally high specific capacitance of 314F/g.

Acknowledgments This work was supported by the Deanship of Scientific Research, Vice Presidency for Graduate Studies and Scientific Research, King Faisal University, Saudi Arabia [Grant No. 5473]. The authors P. A. Alvi and Ravina acknowledge the Department of Science and Technology (DST), Government of India, for awarding the CURIE project to Banasthali Vidyapith, Rajasthan. P. A. Alvi appreciates the DST, Government of India, for granting the STUTI project to Banasthali Vidyapith.

Conflict of interest The authors declare that they have no conflict of interest.

References

1. B. Rani and N.K. Sahu, Electrochemical properties of $CoFe_2O_4$ nanoparticles and its rGO composite for supercapacitor. *Diam. Relat. Mater.* 108, 107978 (2020).
2. N. Budhiraja, V. Kumar, and S.K. Singh, Synergistic effect in structural and supercapacitor performance of well dispersed $CoFe_2O_4/Co_3O_4$ nano-hetrostructures. *Ceram. Int.* 44(12), 13806–13814 (2018).
3. G. Wang, L. Zhang, and J. Zhang, A review of electrode materials for electrochemical supercapacitors. *Chem. Soc. Rev.* 41(2), 797–828 (2012).
4. I. Ayman, A. Rasheed, S. Ajmal, A. Rehman, A. Ali, I. Shakir, and M.F. Warsi, $CoFe_2O_4$ nanoparticle-decorated 2D MXene: a novel hybrid material for supercapacitor applications. *Energy Fuels* 34(6), 7622–7630 (2020).
5. J.S. Shaikh, N.S. Shaikh, R. Kharade, S.A. Beknalkar, J.V. Patil, M.P. Suryawanshi, and P.S. Patil, Symmetric supercapacitor: sulphurized graphene and ionic liquid. *J. Colloid Interface Sci.* 527, 40–48 (2018).
6. J.S. Sagu, K.G.U. Wijayantha, and A.A. Tahir, The pseudocapacitive nature of $CoFe_2O_4$ thin films. *Electrochim. Acta* 246, 870–878 (2017).
7. R. Bhosale, S. Bhosale, V. Chavan, C. Jambhale, D.-k Kim, and S. Kolekar, Hybrid supercapacitors based on nanoporous carbon and $CoFe_2O_4$ derived from a bimetallic organic framework. *ACS Appl. Nano Mater.* 7(2), 2244–2257 (2024).
8. C. Xia, T. Ren, R. Darabi, M. Shabani-Nooshabadi, J.J. Klemeš, C. Karaman, F. Karimi et al., Spotlighting the boosted energy storage capacity of $CoFe_2O_4$/Graphene nanoribbons: a promising positive electrode material for high-energy-density asymmetric supercapacitor. *Energy* 270, 126914 (2023).
9. E. Samuel, B. Joshi, H.S. Jo, Y.I. Kim, S. An, M.T. Swihart, and S.S. Yoon, Carbon nanofibers decorated with FeOx nanoparticles as a flexible electrode material for symmetric supercapacitors. *Chem. Eng. J.* 328, 776–784 (2017).
10. S. Sun, T. Zhai, C. Liang, S.V. Savilov, and H. Xia, Boosted crystalline/amorphous Fe2O3-δ core/shell heterostructure for flexible solid-state pseudo capacitors in large scale. *Nano Energy* 45, 390–397 (2018).
11. H. Hu, B. Guan, B. Xia, and X.W. Lou, Designed formation of $Co_3O_4/NiCo_2O_4$ double-shelled nanocages with enhanced pseudocapacitive and electrocatalytic properties. *J. Am. Chem. Soc.* 137(16), 5590–5595 (2015).
12. Q. Zhao, Z. Yan, C. Chen, and J. Chen, Spinels: controlled preparation, oxygen reduction/evolution reaction application, and beyond. *Chem. Rev.* 117(15), 10121–10211 (2017).
13. S.H. Joo, S.J. Choi, I. Oh, J. Kwak, Z. Liu, O. Terasaki, and R. Ryoo, Ordered nanoporous arrays of carbon supporting high dispersions of platinum nanoparticles. *Nature* 412(6843), 169–172 (2001).
14. C. Zequine, S. Bhoyate, F. Wang, X. Li, K. Siam, P.K. Kahol, and R.K. Gupta, Effect of solvent for tailoring the nanomorphology of multinary $CuCo_2S_4$ for overall water splitting and energy storage. *J. Alloy. Compd.* 784, 1–7 (2019).
15. A. Kumari, K. Kumari, R.N. Aljawfi, P.A. Alvi, S. Dalela, M.M. Ahmad, A.K. Chawla, R. Kumar, A. Vij, and S. Kumar, Role of La substitution on structural, optical, and multiferroic properties of $BiFeO_3$ nanoparticles. *Appl. Nanosci.* 13(5), 3161–3180 (2023).
16. Ravina, S. Kumar, S.Z. Hashmi, G. Srivastava, J. Singh, A.M. Quraishi, S. Dalela, F. Ahmed, and P.A. Alvi, Synthesis and investigations of structural, surface morphology, electrochemical, and electrical properties of NiFe2O4 nanoparticles for usage in supercapacitors." *J. Mater. Sci.: Mater. Electr.* 34(10), 868 (2023).
17. J. Sahu, S. Kumar, P.A. Faheem Ahmed, B. Alvi, D.M. Dalela, M.G. Phase, and S. Dalela, Electrochemical and electronic structure properties of high-performance supercapacitor based on Nd-doped ZnO nanoparticles. *J. Energy Storage* 59, 106499 (2023).
18. S. Dalela, S. Kumar, B.L. Choudhary, and P.A. Alvi, Structural, optical and Raman studies of Co3O4 nano-particles. *Mater. Today: Proc.* 79, 165–168 (2023).
19. U. Ghazanfar, S.A. Siddiqi, and G. Abbas, Study of room temperature dc resistivity in comparison with activation energy and drift mobility of NiZn ferrites. *Mater. Sci. Eng. B* 118(1–3), 132–134 (2005).
20. J. Petzold, Applications of nanocrystalline soft magnetic materials for modern electronic devices. *Scripta Mater.* 48(7), 895–901 (2003).
21. G.A. El-Shobaky, A.M. Turky, N.Y. Mostafa, and S.K. Mohamed, Effect of preparation conditions on physicochemical, surface and catalytic properties of cobalt ferrite prepared by coprecipitation. *J. Alloy. Compd.* 493(1–2), 415–422 (2010).
22. I. Sandu, L. Presmanes, P. Alphonse, and P. Tailhades, Nanostructured cobalt manganese ferrite thin films for gas sensor application. *Thin Solid Films* 495(1–2), 130–133 (2006).
23. L. Lv, Q. Xu, R. Ding, L. Qi, and H. Wang, Chemical synthesis of mesoporous $CoFe_2O_4$ nanoparticles as promising bifunctional electrode materials for supercapacitors. *Mater. Lett.* 111, 35–38 (2013).
24. M. Qorbani, N. Naseri, and A.Z. Moshfegh, Hierarchical $Co_3O_4/Co(OH)_2$ nanoflakes as a supercapacitor electrode: experimental and semi-empirical model. *ACS Appl. Mater. Interfaces* 7(21), 11172–11179 (2015).
25. M. Kim, Oh. Ilgeun, and J. Kim, Effects of different electrolytes on the electrochemical and dynamic behavior of electric double

layer capacitors based on a porous silicon carbide electrode. *Phys. Chem. Chem. Phys.* 17(25), 16367–16374 (2015).
26. G. Lota, K. Fic, and E. Frackowiak, Carbon nanotubes and their composites in electrochemical applications. *Energy Environ. Sci.* 4(5), 1592–1605 (2011).
27. K. Song, X. Chen, R. Yang, B. Zhang, X. Wang, P. Liu, and J. Wang, Novel hierarchical $CoFe_2Se_4$@ $CoFe_2O_4$ and $CoFe_2S_4$@ $CoFe_2O_4$ core-shell nanoboxes electrode for high-performance electrochemical energy storage. *Chem. Eng. J.* 390, 124175 (2020).
28. P.J.G.W.G. Scherrer, Bestimmung der Grösse und der inneren von KolloidteilchenmittelsRöntgenstrahlenStruktur Nachr. *Ges Wiss Göttingen* 26, 98–100 (1918).
29. S.B. Dangi, S.Z. Hashmi, B.L. Upendra Kumar, A.E. Choudhary, S.D. Kuznetsov, S. Kumar et al., Exploration of spectroscopic, surface morphological, structural, electrical, optical and mechanical properties of biocompatible PVA-GO PNCs. *Diam. Relat. Mater.* 127, 109158 (2022).
30. M. Sharma, R.N. Aljawfi, K. Kumari, K.H. Chae, S. Dalela, S. Gautam, P.A. Alvi, and S. Kumar, Investigation of local geometrical structure, electronic state and magnetic properties of PLD grown Ni doped SnO2 thin films. *J. Electr. Spectrosc. Relat. Phenom.* 232, 21–28 (2019).
31. A. Kumari, K. Kumari, F. Ahmed, P.A. Adil Alshoaibi, S.D. Alvi, M.M. Ahmad et al., Influence of Sm doping on structural, ferroelectric, electrical, optical and magnetic properties of $BaTiO_3$. *Vacuum* 184, 109872 (2021).
32. G. Srivastava, S. Kumar, S.Z. Hashmi et al., Study of structural, surface morphology, Raman spectroscopy, and electrochemical properties of $Bi_{1+x}FeO_3$ nanoparticles for usage in supercapacitors. *Opt. Quant. Electron.* 55, 1235 (2023).